HHS Public Access

Author manuscript

Biomaterials. Author manuscript; available in PMC 2016 December 01.

Published in final edited form as:

Biomaterials. 2015 December ; 73: 85–95. doi:10.1016/j.biomaterials.2015.09.005.

Substrate Modulus of 3D-Printed Scaffolds Regulates the Regenerative Response in Subcutaneous Implants through the Macrophage Phenotype and Wnt Signaling

R Guo[1], **AR Merkel**[2,3,4], **JA Sterling**[2,3,4,5], **JM Davidson**[2,6], and **SA Guelcher**[1,3,7]

[1] Department of Chemical and Biomolecular Engineering, Vanderbilt University, Nashville, TN, 37235, USA

[2] Research Service, Department of Veterans Affairs Tennessee Valley Healthcare System, Nashville, TN, 37212, USA

[3] Center for Bone Biology, Vanderbilt University Medical Center, Nashville, TN, 37232, USA

[4] Division of Clinical Pharmacology, Department of Medicine, Vanderbilt University Medical Center, Nashville, TN, 37232, USA

[5] Department of Cancer Biology, Vanderbilt University Medical Center, Nashville, TN, 37232, USA

[6] Department of Pathology, Immunology, and Microbiology, Vanderbilt University, Nashville, TN 37232, USA

[7] Department of Biomedical Engineering, Vanderbilt University, Nashville, TN, 37235, USA

Abstract

The growing need for therapies to treat large cutaneous defects has driven recent interest in the design of scaffolds that stimulate regenerative wound healing. While many studies have investigated local delivery of biologics as a restorative approach, an increasing body of evidence highlights the contribution of the mechanical properties of implanted scaffolds to wound healing. In the present study, we designed poly(ester urethane) scaffolds using a templated-Fused Deposition Modeling (t-FDM) process to test the hypothesis that scaffolds with substrate modulus comparable to that of collagen fibers enhance a regenerative versus a fibrotic response. We fabricated t-FDM scaffolds with substrate moduli varying from 5 – 266 MPa to investigate the effects of substrate modulus on healing in a rat subcutaneous implant model. Angiogenesis, cellular infiltration, collagen deposition, and directional variance of collagen fibers were maximized for wounds treated with scaffolds having a substrate modulus (K_s = 24 MPa) comparable to that of collagen fibers. The enhanced regenerative response in these scaffolds was correlated with down-regulation of Wnt/β-catenin signaling in fibroblasts, as well as increased polarization of macrophages toward the restorative M2 phenotype. These observations highlight the substrate modulus of the scaffold as a key parameter regulating the regenerative versus scarring

Correspondence to: SA Guelcher.

phenotype in wound healing. Our findings further point to the potential use of scaffolds with substrate moduli tuned to that of the native matrix as a therapeutic approach to improve cutaneous healing.

Keywords

scaffold; wound healing; macrophage polarization; Wnt signaling; elastic modulus; fibroblast

1. Introduction

The growing need for the treatment of large cutaneous defects has led to considerable interest in the design of improved scaffolds for stimulating wound healing. While many studies have focused on the acceleration of wound closure, a growing number of studies have aimed to restore the function of impaired tissue through a more restorative wound approach [1]. Local delivery of recombinant human (rh) growth factors, such as platelet-derived growth factor (rhPDGF), transforming growth factor-β (rhTGF-β), and vascular endothelial growth factor (rhVEGF), from scaffolds has improved wound repair and restoration [2-4]. However, growth factor delivery requires optimized release kinetics to enhance tissue healing and minimize adverse events [5], and translation of local drug delivery technologies to the clinic requires a more complex regulatory pathway.

An increasing body of evidence highlights the contribution of the mechanical properties of implanted scaffolds to wound healing [6, 7]. The elastic modulus of the scaffold influences scar formation through both the organization of fibroblasts infiltrating the wound bed as well as the abundance and orientation of extracellular matrix they deposit [8, 9]. The mechano-responsive properties of fibroblasts, which comprise a significant component of granulation tissue, have been investigated to understand the mechanisms by which elastic modulus regulates wound healing. Mechanical forces experienced by dermal fibroblasts, either through applied strain [10] or a stiff extracellular substrate [11], activate the Wnt/β-catenin signaling pathway, which promotes the fibroblast-myofibroblast transition [12, 13] and is required for TGF-β-mediated fibrosis [14-16]. Genetically stabilized β-catenin can lead to hypertrophic scars [17-19], and thus down-regulation of the elevated β-catenin protein level of wound fibroblasts [19] is required to improve cutaneous wound repair.

In addition to Wnt signaling, macrophage polarization has also been implicated as a factor regulating the regenerative versus fibrotic phenotype. Recent studies have reported that both M1 and M2 macrophage phenotypes are present throughout the wound healing process, but the relative ratio of regenerative (M2) to inflammatory (M1) macrophages contributes to wound healing outcomes [20, 21]. Markers for M1 and M2 macrophages have been quantified in unfractionated cells harvested from wounds to determine their influence on wound healing [22, 23]. Several physical factors have been reported to regulate macrophage polarization, including cell shape [24], scaffold pore size [25, 26], and mechanical forces applied to scaffolds, which stimulate inflammation through activation of focal adhesions [18, 27] and integrins [28]. However, the effects of substrate modulus on macrophage polarization have not been extensively investigated [29, 30].

In the present study, we designed poly(ester urethane) scaffolds using a templated-Fused Deposition Modeling (t-FDM) process to investigate the effects of the modulus of the polymeric substrate (referred to as the substrate modulus K in contrast to the bulk modulus of the scaffold K^*) on wound healing in a rat subcutaneous model. Three values of substrate modulus were investigated: 5 MPa (less rigid than a collagen fiber), 24 MPa (comparable to a collagen fiber (32 MPa [31])), and 266 MPa (more rigid than a collagen fiber). Previous studies have reported that regeneration is enhanced under conditions where (1) the bulk modulus of the scaffold (K^*) exceeds that of host dermal tissue (0.05 MPa) [32], and (2) the scaffold perists throughout all stages of the remodeling process [1]. In order to isolate the effects of substrate modulus on healing, t-FDM scaffolds with $K^* \geq 0.5$ MPa were fabricated using a slow-degrading polymer composition (5 – 10% mass loss at 3 weeks [33]). We hypothesized that scaffolds with substrate moduli approaching that of a collagen fiber would enhance the regenerative versus the fibrotic response. The effects of substrate modulus on collagen deposition and alignment, angiogenesis, Wnt signaling, and macrophage polarization were investigated in a rat subcutaneous model.

2. Materials and Methods

2.1 Materials

DMEM (1.0 g/L glucose = 1.0 g/L) and fetal bovine serum (FBS) were purchased from Thermo Scientific. Penicillin/streptomycin (P/S), trypsin EDTA, and Amphotericin B were obtained from Corning Cellgro. Glycolide and D,L-lactide were purchased from Polysciences (Warrington, PA). Hexamethylene diisocyanate trimer (HDIt) was supplied by Bayer Material Science (Pittsburgh, PA). Iron acetylacetonate (FeAA) catalyst was supplied by Sigma-Aldrich. ε-caprolactone (Sigma-Aldrich) was dried over anhydrous $MgSO_4$, and all other materials were used as received.

2.2 Fabrication of scaffolds from 3D printed PLA templates

Polylactic acid (PLA) templates were designed by Solidworks (Waltham, MA) with desired fiber diameter and dimensions and then fabricated by Fused Deposition Modeling (FDM) with a MakerBot® Replicator® 2 3D printer. Polyester triols (300 g/mol, 720 g/mol or 3000 g/mol) were synthesized from a glycerol starter and a backbone comprising ε-caprolactone (70 mol-%), glycolide (20 mol-%), and D,L-lactide (10 mol-%) as described previously [34]. This composition was selected due to its slow degradation time ($t_{1/2}$ > 200 days [35]). Dried glycerol, ε-caprolactone, glycolide, D,L- lactide, and 45 μL stannous octoate were mixed in a 100 mL flask and heated under an argon atmosphere with mechanical stirring to 130°C. After a reaction time of 24 h, the mixture was removed from the heater and washed with hexane. Poly(ester urethane) scaffolds were synthesized by reactive liquid molding of HDIt with a hardener component comprising the polyester triol and iron catalyst (5% iron acetylacetonate (FeAA) in dipropylene glycol). The reactants were poured into the PLA templates (for 3D scaffolds) or tissue culture plates (for 2D films) after mixing. Both the filled 3D PLA templates and tissue culture plates (2D films) were cured at 60°C overnight. After cure, the PLA template was leached from the scaffold by immersion in dichloromethane overnight.

2.3 Scaffold characterization

Scaffold porosity was calculated from mass and volume measurements of cylindrically punched 3D scaffolds (n=4) as previously described [34]. Pore size and morphology of the scaffolds were measured by scanning electron microscopy (Hitachi S-4200 SEM, Finchampstead, UK) after gold sputter coating with a Cressington Sputter Coater. The bulk moduli of both the 2D films (K_f) and 3D scaffolds (K^*) were measured under compression by MTS after pre-soaking in PBS overnight at 37°C [36]. To confirm that the substrate modulus is the same for the polymer in both the 2D films and 3D scaffolds, the bulk modulus of the polymeric substrate in the 3D scaffolds ($K_{s,pred}$) was calculated from measured values of K^*, polymer density (ρ = 1.27 g cm^{-3}), and scaffold porosity ε (52.9 ± 2%) [37]:

$$K_{s,pred} = K^* \left(\frac{\rho}{1 - \rho\varepsilon} \right)^2 \quad (1)$$

2.4 In vivo cutaneous repair in rats

All surgical and care procedures were carried out under aseptic conditions per an approved Institutional Animal Care and Use Committee (IACUC) protocol. The study design is listed in Table 1. Scaffolds (n=4) were punched into 6-mm diameter cylinders, sliced to form 2-mm thick discs, and implanted in subcutaneous pockets in adult male Sprague-Dawley rats to induce granulation tissue formation. All scaffolds were sterlized in 70% ethanol overnight and washed with PBS prior to implantation. Rats were euthanized 7d, 14d, and 21d after surgery and the implants harvested for histology and quantitative real-time PCR (qRTPCR). For histological staining, harvested implants were fixed in neutral buffered formalin overnight, dehydrated in an EtOH series, embedded in paraffin, and sectioned at 5 μm. Cellular infiltration was quantified by hematoxylin & eosin (H&E) performed on the tissue sections. Histological images were taken by Olympus light microscope, and image analysis was performed with Image J. Cell types were identified based upon their staining and morphology: neutrophils were round and purple with multilobular nuclei; monocytes were large, round, and purple; and fibroblasts were spindle-shaped and purplish-blue. Tissue sections were also stained with Masson's trichrome green, which stains host collagen dark green, host muscle dark red, new extracellular matrix and collagen fibers emerald green, erythrocytes red, and cytoplasm of infiltrating cells pinkish-red. Collagen fiber orientation was measured from tissue sections stained with Masson's trichrome green, and color images were taken under standardized settings. The fiber alignment evaluation was carried out using the ImageJ plug-in “OrientationJ” [38, 39]. Collagen fiber directional variance of infiltrated tissues was calculated from the local angle distribution by analyzing the low magnification images (2x) at each pixel using coherency-weighted alignment. To compare the local fiber alignment, directional variance was computed and normalized to the total pixels of the selected region of interest.

2.5 Isolation and culture of fibroblasts

Primary rat fibroblasts from granulation tissue were generated from pooled, implanted scaffolds from 4 rats and were maintained in DMEM supplemented with 10% FBS, 1%

Penicillin/Streptomycin, and 0.1% Amphotericin B (Sigma). Primary rat dermal fibroblasts were isolated by skin explant culture as previously described [40]. Briefly, rat skin was harvested and incubated in trypsin-EDTA (0.25%EDTA, phenol red) overnight at 4°C, and the dermis was detached from other tissues, minced, and plated in a tissue culture plate with complete cell culture medium. Cells were detached at sub-confluency by trypsin-EDTA, re-suspended at 10^5 cells/mL in complete medium, and cultured on 12-well tissue culture plates (1 mL/well) or on 2D films with varying substrate modulus in 6-well plates. To facilitate cell attachment, all poly(ester urethane) 2D films were pretreated with fibronectin (4 μg/mL in PBS) at 37°C for 24 h. Fibroblasts (either dermal or from granulation tissue) were plated on 2D films and cultured in complete medium for up to 7 d. Cells were detached by trypsin EDTA (0.25%) and total protein extracted from cell pellets by RIPA buffer (Thermo Scientific) containing protease inhibitors and phosphatase inhibitors (Thermo) on ice for 15 min. Protein concentration was measured by Pierce BCA Protein Assay Kit.

2.6 Western Blotting

Equal amounts of total protein from cell lysates were loaded onto SDS-PAGE gels, separated by Bio-Rad 2-D Electrophoresis units, and transferred to PVDF membranes. The membrane was blocked in LI-COR preformed blocking buffer for 1h at room temperature and then incubated with β-catenin antibody (8480S, Cell Signaling) in blocking buffer at 4°C with gentle shaking overnight. HRP-conjugated goat anti-rabbit secondary antibody was then applied to the membranes after washing, and signals were detected by chemiluminescence (Western Lightning Plus ECL, Perkin Elmer).

2.7 Gene Expression by qRTPCR

Harvested tissue samples were maintained in RNALater buffer until ready for RNA extraction. Total RNA was isolated from the harvested scaffolds or cell pellets by RNeasy mini Kit (Qiagen). cDNA synthesis was carried out from purified total RNA using iScript™ Reverse Transcription Supermix (Bio-Rad). qRTPCR products amplified for growth factors (*PDGF-BB, Tgfb1, Pecam1(CD31) and Vegfa*), collagens (*Col1A1 and Col3A1*), macrophages (Nos2 (*iNOS), Mrc1 (CD206) and TNF*), and Wnt/β-catenin signaling pathway-related genes (*sFRP2, Ccnd1 (CyclinD1), and Axin2*) were measured to compare the effects of substrate modulus on wound healing. The primers used for qRTPCR amplification are listed in Table 2. qRTPCR was performed with the IQ Real Time SybrGreen PCR Supermix (Bio Rad). All reactions were run in triplicate, and the qRTPCR results of all genes were normalized to GAPDH.

2.8 Immunohisochemical staining

Formalin-fixed, paraffin-embedded tissues were sectioned at 5 μm, placed on slides, and warmed overnight at 60°C. Slides were deparaffinized and rehydrated with graded alcohols ending in Tris buffered saline (TBS-T Wash Buffer, LabVision, Freemont, CA). Heat-mediated target retrieval was performed in 1X Target Retrieval Buffer (Citrate, pH 6.0, DAKO, Carpenteria, CA). Endogenous peroxidases and non-specific background were blocked by subsequent incubations in 3% H_2O_2 (Fisher, Suwanee, GA) in TBS-T and protein block (DAKO). Primary antibodies to rat CD68 (Bio-Rad,1:800), CD31 (AbDSerotec, 1:100), Collagn IV (Abcam, 1:600), and Ki67 (Abam, 1:100) for 1 h followed

by secondary incubation and tertiary incubation in SA-HRP (RTU, BD Pharmingen, San Jose, CA). Slides were rinsed with TBS-T between each reagent treatment and all steps were carried out at room temperature. Visualization was achieved with DAB+ chromogen (DAKO). Slides were counterstained with Mayer's hematoxylin, dehydrated through a series of alcohols and xylenes, and then coverslipped with Acrytol Mounting Media (Surgipath, Richmond, IL). Immunohistochemical staining was performed usingBond Max Autostainer (Leica).

2.9 Immunofluorescence staining

To confirm that the effects of substrate rigidity on the number of $Ki67^+$ fibroblasts were comparable for 2D films and 3D scaffolds, fibroblasts (10^5/film) isolated from the granulation tissue were cultured on 2D-5, 2D-24, and 2D-266 films cast in 12-well tissue culture plates. There were no statistical differences in the number of cells attached to each film at 16 hours post-seeding as determined by a total protein assay. After 3 days of culture, cells were fixed in 4% Formaldehyde and blocked in Odyssey blocking buffer (PBS) (diluted one time in PBS-T) for 1 h. For Ki67 detection, fixed cells were incubated with Ki67 antibody (Vector, 1:1000) at room temperature for 1 h, and an Alexa Fluor® 488-tagged secondary antibody was applied. Images were obtained with a 20x objective on an Olympus BX41 upright microscope. The number of positively stained cells at day 3 was measured for each film from 6 fields of view observed with a 40X objective.

2.9 Statistical analysis

The statistical significance between experimental groups was determined by one-way ANOVA with Bonferroni correction. Graphs show means ± SEM, and $p < 0.05$ is considered as statistically significant.

3 Results

3.1 Fabrication of templated 3D scaffolds

We investigated the effects of substrate modulus on rat subcutaneous wound healing. To ensure that the mechanical properties of the scaffold did not change over the time course of the experiment, HDIt was selected as the isocyanate component because of its relatively slow hydrolytic degradation rate compared to the time scale of wound healing [41]. Considering the limited number of materials available for FDM, we printed PLA templates with a MakerBot® Replicator®2 3D printer (Figure 1A) and filled them with a reactive poly(ester urethane) with tunable substrate modulus. We used polyester triols with molecular weights of 3000, 720, and 300 g mol^{-1} to prepare poly(ester urethane) networks with substrate moduli of 5, 24, and 266 MPa, respectively (Figure 1B). For each polymer composition, there was no significant difference between the measured substrate moduli of the 2D films (K_f) and the substrate moduli of the polymeric substrate in the 3D scaffolds calculated from Eq (1) ($K_{s,pred}$). Thus, the substrate modulus of a given polymeric composition was comparable for both 2D films and 3D scaffolds (Figure 1B). Leaching of the PLA template in dichloromethane yielded scaffolds with interconnected pores and a pore diameter of 423 ± 34 μm (Figure 1C).

3.2 Effects of substrate modulus on cellular infiltration in a rat subcutaneous wound model

In order to investigate the effects of substrate modulus on wound healing, 3D-5, 3D-24, and 3D-266 scaffolds (Figure 1B) were implanted subcutaneously in adult male Sprague-Dawley rats. Scaffolds were explanted for histological analysis at d7, d14, and d21, and cellular infiltration between different groups was compared by H&E staining. Infiltrating cells included inflammatory cells (e.g., neutrophils and monocytes/macrophages) and fibroblasts (Figure 2A), and the area-% infiltrating cells was highest on 3D-24 scaffolds (measured by histomorphometry, Figure 2B). Cell proliferation within the wound bed was analyzed by Ki67 immunohistological staining and quantified by the area-% $Ki67^+$ cells. Similar to the trend observed for cellular infiltration, the population of $Ki67^+$ cells remained significantly higher in the 3D-24 scaffolds compared to the other two groups up to d14 (Figure 2C). $Ki67^+$ cells decreased in all three groups after d14, and no significant differences were observed among the three groups. These observations suggest that the 3D-24 scaffolds preferentially stimulated cell proliferation and infiltration during the early stages of wound healing.

3.3 Effects of substrate modulus on matrix deposition and alignment in a rat subcutaneous wound model

Collagen deposition in the wound bed was analyzed by trichrome green staining. High-magnification images of histological sections showed increased deposition of new collagen fibers and extracellular matrix (stained emerald green) in the 3D-24 scaffolds on d7 (Figure 3A). In addition, expression of both types I and III collagen (*Col1A1* and *Col3A1*) measured by qRTPCR correlated with the histological findings, in which both *Col1A1* and *Col3A1* expression were greatest in 3D-24 scaffolds (Figure 3B-C). To compare differences in scarring between groups, the alignment of fibroblasts and deposited collagen fibers was evaluated as previously described [42]. Both quantitative (Figure 3D) and qualitative (Figure 3E) data illustrate alignment of the cells and extracellular matrix for each of the treatment groups. At each time point, directional variance values were significantly more disordered for the 3D-24 scaffolds compared to the 3D-5 and 3D-266 scaffolds (Figure 3D). Figure 3E shows the collagen angular distribution. Both 3D-5 and 3D-266 scaffolds showed a lower degree of random orientation (lack of variance as evidenced by a linear alignment of cells and collagen fibers) than 3D-24 scaffolds, which displayed a higher degree of random orientation. Directional variance of collagen fibers was the largest in the 3D-24 scaffolds, indicating random alignment of collagens rather than linear scarring.

3.4 Effects of substrate modulus on expression of growth factors associated with vascularization and wound healing

To understand the molecular mechanism of how substrate modulus affects wound healing, we measured expression of three growth factors that are closely related to cutaneous wound repair *in vivo*: PDGF, TGF-β1, and VEGF. Considering previous studies highlighting the importance of PDGF in wound healing and reporting that reduced expression of PDGF was observed in an impaired animal wound model [43], we first evaluated the expression level of *Pdgfb* gene among all the scaffold groups. As shown in Figure 4A, *Pdgfb* expression in

granulation tissue was significantly higher on 3D-24 scaffolds compared to the other groups up to d21. Expression of *Tgfb1*, which is another key growth factor dominant in wound healing and up-regulated during the healing process [44], was comparable to the other groups at earlier time points but significantly higher on 3D-24 scaffolds on d21 (Figure 4B). In contrast, expression of *Vegfa*, which is highly involved in vascularization during wound healing [45], was characterized by lower expression in the 3D-24 scaffolds (Figure 4C).

The effects of substrate modulus on angiogenesis were also evaluated in this study. Gene expression of *Pecam1* (CD31) was evaluated as a marker of neovessel formation [46], and was greatest on 3D-24 scaffolds on d14 and d21 (Figure 4D). IHC showed positive staining for collagen IV present in the endothelial basal lamina [47] (black arrows in Figure 4E). Histomorphometric analysis of Collagen IV staining (Figure 4F) showed that by d21 angiogenesis in the wound bed was significantly higher in 3D-24 scaffolds, which was consistent with *Pecam1* gene expression data.

3.5 Effects of substrate modulus on expression of Wnt-related genes by fibroblasts infiltrating the wound bed

Differences in cellular infiltration, matrix deposition, and gene expression as a function of substrate modulus point to a mechanotransduction mechanism regulating wound healing. Wnt signaling has been recognized as a key mechanotransduction pathway in fibroblasts that regulates wound healing [10, 11]; therefore, the expression level of Wnt-related genes by fibroblasts in response to substrate rigidity was evaluated. Since fibroblasts have been reported to be highly mechanosensitive [48] and infiltrate the scaffold during cutaneous wound repair, the effects of substrate modulus on fibroblasts isolated from the granulation tissue were investigated. Fibroblasts harvested from the implanted scaffolds at d7 were plated on 2D-5, 2D-24, and 2D-266 films with substrate moduli comparable to those of the corresponding 3D scaffolds (Figure 1B). Expression of Wnt-related target genes *Ccnd1* (cyclin D1) and *Axin2* was lowest on 3D-24 scaffolds, while expression of secreted Frizzled-Related Protein-2 (*sFRP2*, an inhibitor of Wnt signaling) was highest on 3D-24 scaffolds (Figure 5A). Moreover, protein expression level of β-catenin, an intracellular signal transducer in the Wnt signaling pathway, as well as its target protein Cyclin D1, were also lowest on 3D-24 scaffolds (Figure 5B-D). To confirm that the effects of substrate modulus on the number of $Ki67^+$ cells on 2D films and 3D scaffolds (Figure 2C) were comparable, Ki67 immunofluorescence staining was performed on fibroblasts (10^5/film) cultured on 2D-5, 2D-24, and 2D-266 films (Figure 5E-F) after 3 days culture. Consistent with the *in vivo* analysis for implanted 3D scaffolds (Figure 2C), the number of $Ki67^+$ cells was highest on 2D-24 films.

3.6 Effects of substrate modulus on macrophage polarization (M1/M2 ratio)

Considering that polarization of macrophages is critical for wound repair and regeneration [49], we investigated the effects of substrate modulus on macrophage polarization. Expression of *Nos2* (iNOS) was selected as a marker for the M1 inflammatory phenotype, and *Mrc1* (CD206, mannose receptor 1) were selected as a marker for the M2 regenerative phenotype [50]. Expression of *Nos2* was highest (Figure 6A) and expression of *Mrc1* lowest (Figure 6B) on 3D-266 scaffolds. Therefore, the macrophage polarization ratio M1/M2,

which determines the inflammatory versus reparative potential during wound healing, was lowest in 3D-24 scaffolds at d7 (Figure 6C). Similarly, expression of the inflammatory cytokine *Tnf*, which is associated with the M1 phenotype, was lower on 3D-5 and 3D-24 scaffolds (Figure 6D). Immunohistochemical staining for CD68, a pan-macrophage marker, was performed to determine the total macrophage population (Figure 6E-F). $CD68^+$ macrophages (brown; arrows in Figure 6F) were concentrated near the surface of the residual scaffold (S). Similar to the gene expression data, the total number of $CD68^+$ macrophages was lowest in 3D-24 scaffolds. Both the macrophage polarization and abundance data suggest that the 3D-24 scaffolds polarize infiltrating macrophages toward the regenerative phenotype, which is consistent with the matrix deposition/alignment, angiogenesis, and Wnt signaling pathway data.

4 Discussion

Cutaneous tissue repair in adults is an imperfect compromise between regenerative repair and restoration of integrity [51]. Scaffolds, whether biological or synthetic, offer the prospect of creating a favorable physical and chemical environment for tissue restoration. Scaffold pore size, morphology, and interconnectivity [52, 53] as well as the scaffold degradation rate [1, 54] can potentially reduce scar formation; however, the effects of substrate modulus on matrix deposition and alignment, angiogenesis, and macrophage phenotype have been less extensively investigated. Mechanical stress can have beneficial effects on cutaneous regeneration via enhanced proliferation, angiogenesis, and stem cell recruitment [55], but it also increases infiltration of inflammatory cells and decreases apoptosis of local cells involved in wound remodeling, both of which are major factors in tissue fibrosis and scarring [56]. These competing effects suggest that there may be an optimal substrate modulus that promotes the regenerative versus the scarring phenotype. In order to isolate the effects of substrate modulus on wound healing, we applied the t-FDM technique to precisely control the properties of the scaffolds. High interconnectivity was achieved at 50% porosity, which enabled the fabrication of scaffolds with bulk moduli exceeding that of dermal tissue and therefore effective space maintenance [32]. Furthermore, t-FDM scaffolds were prepared from polymers that persist throughout the remodeling phase [33], a property that has been reported to favor regeneration versus scarring [1]. We designed scaffolds with substrate moduli ranging from 5 – 266 MPa to investigate the effects of substrate modulus on cutaneous wound healing. Scaffolds with a substrate modulus comparable to that of collagen fibers (24 MPa) promoted increased deposition and random orientation of collagen, angiogenesis, and regenerative macrophage polarization compared to scaffolds more compliant (5 MPa) or rigid (266 MPa) than collagen fibers. Additionally, Wnt signaling was down-regulated on 3D-24 scaffolds. These observations point to substrate modulus as a key parameter regulating a regenerative versus a scarring phenotype.

Many growth factors, such as PDGF [43], TGF-β1 [44], and VEGF [45], have been shown to be critical for cutaneous wound repair. To better understand the mechanism of how substrate modulus affects wound healing, we evaluated the expression level of these growth factors in the total RNA extracted from infiltrated scaffolds at d7, d14, and d21. PDGF-BB expression was up-regulated in the 3D-24 scaffolds, which was consistent with the elevated infiltration, proliferation and vascularity findings. Up-regulation of PDGF by infiltrating cells is

essential for enhanced cutaneous wound healing [43], and exogenous PDGF increases volume and cell density of granulation tissue but not the extracellular components or epidermal growth [57]. Interestingly, VEGF expression was low on 3D-24 scaffolds and did not correlate with neovascularization (indicated by *Pecam1* expression and collagen IV IHC). While these observations are surprising, previous studies have suggested that the effects of VEGF on wound closure may depend on the type of wound. Thus, increased expression of VEGF contributed to expedient closure in large excisional wounds [45], but neutralization of VEGF significantly reduced scar size and enhanced the quality of the collagen deposited in incisional wounds [55]. TGF-β1 is another important growth factor for wound regeneration, and has been reported to promote cellular infiltration and proliferation at wound sites [44]. However, it is a major factor in the expression of collagens and the myofibroblastic differentiation of fibroblasts. In the present study, the expression level of TGF-β1 in 3D-24 scaffolds was significantly higher than the other two groups at d21. However, these studies did not determine the level of TGF-β1 activation, which is strongly influenced by cell-matrix interactions [58], and thus the effects of substrate rigidity on TGF-β1 activation and wound healing warrant further investigation.

The similarity of growth factor expression levels in total RNA directly harvested from granulation tissue or dermal fibroblasts points to these cells as mediators of the effects of substrate rigidity on wound healing. Among the mechanotransduction pathways, the Wnt/β-catenin pathway has been reported to be crucial for cutaneous wound regeneration [17-19], while abnormally elevated β-catenin in wound fibroblasts is considered to contribute to excessive fibrosis and scar formation [59, 60]. The response of this pathway to substrate rigidity was therefore evaluated in fibroblasts. Granulation tissue-derived fibroblasts showed down-regulated Wnt signaling on 2D-24 films, as evidenced by decreased expression of the target genes *Ccn2* and *Axin2*, decreased β-catenin and cyclin D1 protein production, and increased expression of the Wnt inhibitor *sFRP2* (Figure 5A-B). The number of $Ki67^+$ proliferating cells was highest on both 3D-24 (Figure 2C) scaffolds and 2D-24 films (Figure 5E-F), which contrasted with the cyclin D1 trend (Figure 5A-B). While cyclin D1 has been used as a cell cycle indicator, it is also a Wnt target. In contrast, Ki67 is not Wnt-regulated and is strictly associated with cell proliferation [61]. Considering previous studies reporting that the behavior of wound fibroblasts may differ from that of normal dermal fibroblasts [62], we harvested dermal fibroblasts from adult rat skin and verified β-catenin protein expression in response to substrate modulus. Dermal fibroblasts (Figure 5D) exhibited the same minimization of Wnt/β-catenin signaling on 2D-24 films as those harvested from the granulation tissue in the scaffolds (Figure 5B-C). Targeting the Wnt/β-catenin signaling pathway has been considered a potential strategy for the treatment of fibrosis [63], and previous studies have shown that a lower level of β-catenin resulted in smaller wound size [64]. In addition, both sFRP2 overexpression and chemical Wnt inhibitors favor a regenerative response in cutaneous and cardiac repair [65, 66]. Therefore, as an alternative to the delivery of inhibitor molecules of Wnt/β-catenin signaling, our observations highlight the possibility of modulating Wnt/β-catenin signaling in cutaneous wounds by tuning the substrate modulus of the scaffold.

Manipulating the inflammatory macrophage phenotype can also enhance regeneration, in part by altering the fibrotic response. The macrophage phenotype can be regulated by

pharmacological treatment, macrophage-fibroblast interactions, and mechanical and topological properties of the scaffold [25, 26]. Thus, we also investigated the effects of substrate modulus on macrophage polarization in the rat subcutaneous implant model. IHC staining for total macrophages (CD68) showed fewer macrophages in the 3D-5 and 3D-24 scaffolds together with a higher expression level of TNF-α, a pleiotropic cytokine that plays a central role in inflammation and immune system development. A reduced inflammatory response is one of the factors required for scarless wound healing [67], and therefore the reduction in total macrophages in the 3D-24 scaffolds potentially benefits cutaneous wound healing in this study. Recent studies have reported that M1 (inflammatory) and M2 (regenerative) macrophage phenotypes and their relative ratio determines the stage of wound healing [21]. The proportion of cells bearing M1 and M2 markers has been related to healing outcomes [22, 23], and a similar evaluation was conducted in the present study. The M1 marker iNOS was expressed least on 3D-24 scaffolds (Figure 6A), while expression of CD206, an M2 marker, was highest on 3D-24 scaffolds (Figure 6B). Consequently, the M1/M2 ratio was minimized for the 3D-24 scaffolds, suggesting that these scaffolds drive the wound healing response toward regeneration.

5 Conclusions

In this study, we designed t-FDM scaffolds with substrate moduli varying from 5 – 266 MPa to investigate the effects of substrate modulus on healing in a rat subcutaneous implant model. We found that cellular infiltration, collagen deposition and directional variance, and angiogenesis were maximized for wounds treated with 3D-24 scaffolds having a substrate modulus (24 MPa) comparable to that of collagen fibers. An enhanced regenerative response in the 3D-24 scaffolds was correlated with down-regulation of Wnt/β-catenin signaling in fibroblasts as well as increased polarization of macrophages toward the restorative phenotype. These observations highlight the substrate modulus of the implanted scaffold as a key parameter regulating the regenerative versus scarring phenotype in wound healing. Our findings further point to the potential use of scaffolds with substrate moduli tuned to that of collagen fibers as a therapeutic approach to improve cutaneous healing.

Acknowledgments

Research reported in this publication was supported by the National Institute of Arthritis and Musculoskeletal and Skin Diseases under Award Number AR056138, the National Cancer Institute under Award Number CA163499, and the Department of Veterans Affairs, including Award Number 1I01BX001957. The content is solely the responsibility of the authors and does not necessarily represent the official views of the National Institutes of Health or the Department of Veterans Affairs.

References

1. Lorden ER, Miller KJ, Bashirov L, Ibrahim MM, Hammett E, Jung Y, et al. Mitigation of hypertrophic scar contraction via an elastomeric biodegradable scaffold. Biomaterials. 2015; 43:61–70. [PubMed: 25591962]
2. Li B, Davidson JM, Guelcher SA. The effect of the local delivery of platelet-derived growth factor from reactive two-component polyurethane scaffolds on the healing in rat skin excisional wounds. Biomaterials. 2009; 30:3486–94. [PubMed: 19328544]

3. Ashraf A, Lee PH, Kim K, Zaporojan V, Bonassar L, Valentini R, et al. Effect of sustained-release PDGF and TGF-beta on cyclophosphamide-induced impaired wound healing. Plast Reconstr Surg. 2009; 124:1118–24. [PubMed: 19935295]
4. Pandit A, Ashar R, Feldman D. The effect of TGF-beta delivered through a collagen scaffold on wound healing. J Invest Surg. 1999; 12:89–100. [PubMed: 10327078]
5. Richardson TP, Peters MC, Ennett AB, Mooney DJ. Polymeric system for dual growth factor delivery. Nature Biotech. 2001; 19:1029–34.
6. Singer AJ, Clark RA. Cutaneous wound healing. N Engl J Med. 1999; 341:738–46. [PubMed: 10471461]
7. Cao TV, Hicks MR, Standley PR. In vitro biomechanical strain regulation of fibroblast wound healing. The Journal of the American Osteopathic Association. 2013; 113:806–18. [PubMed: 24174502]
8. Smitha B, Donoghue M. Clinical and histopathological evaluation of collagen fiber orientation in patients with oral submucous fibrosis. Journal of oral and maxillofacial pathology : JOMFP. 2011; 15:154–60. [PubMed: 22529573]
9. McDougall S, Dallon J, Sherratt J, Maini P. Fibroblast migration and collagen deposition during dermal wound healing: mathematical modelling and clinical implications. Philosophical transactions Series A, Mathematical, physical, and engineering sciences. 2006; 364:1385–405.
10. Huang C, Miyazaki K, Akaishi S, Watanabe A, Hyakusoku H, Ogawa R. Biological effects of cellular stretch on human dermal fibroblasts. Journal of plastic, reconstructive & aesthetic surgery : JPRAS. 2013; 66:e351–61. [PubMed: 24055333]
11. Barbolina MV, Liu Y, Gurler H, Kim M, Kajdacsy-Balla AA, Rooper L, et al. Matrix rigidity activates Wnt signaling through down-regulation of Dickkopf-1 protein. J Biol Chem. 2013; 288:141–51. [PubMed: 23152495]
12. Kendall RT, Feghali-Bostwick CA. Fibroblasts in fibrosis: novel roles and mediators. Frontiers in pharmacology. 2014; 5:123. [PubMed: 24904424]
13. Liu J, Wang Y, Pan Q, Su Y, Zhang Z, Han J, et al. Wnt/beta-catenin pathway forms a negative feedback loop during TGF-beta1 induced human normal skin fibroblast-to-myofibroblast transition. Journal of dermatological science. 2012; 65:38–49. [PubMed: 22041457]
14. Akhmetshina A, Palumbo K, Dees C, Bergmann C, Venalis P, Zerr P, et al. Activation of canonical Wnt signalling is required for TGF-beta-mediated fibrosis. Nature communications. 2012; 3:735.
15. Zhang DL, Gu LJ, Liu L, Wang CY, Sun BS, Li Z, et al. Effect of Wnt signaling pathway on wound healing. Biochem Biophys Res Commun. 2009; 378:149–51. [PubMed: 19013436]
16. Hamburg EJ, Atit RP. Sustained beta-catenin activity in dermal fibroblasts is sufficient for skin fibrosis. J Invest Dermatol. 2012; 132:2469–72. [PubMed: 22622416]
17. Bielefeld KA, Amini-Nik S, Alman BA. Cutaneous wound healing: recruiting developmental pathways for regeneration. Cellular and molecular life sciences : CMLS. 2013; 70:2059–81. [PubMed: 23052205]
18. Januszyk M, Wong VW, Bhatt KA, Vial IN, Paterno J, Longaker MT, et al. Mechanical offloading of incisional wounds is associated with transcriptional downregulation of inflammatory pathways in a large animal model. Organogenesis. 2014; 10:186–93. [PubMed: 24739276]
19. Cheon SS, Cheah AY, Turley S, Nadesan P, Poon R, Clevers H, et al. beta-Catenin stabilization dysregulates mesenchymal cell proliferation, motility, and invasiveness and causes aggressive fibromatosis and hyperplastic cutaneous wounds. Proc Natl Acad Sci U S A. 2002; 99:6973–8. [PubMed: 11983872]
20. Novak ML, Koh TJ. Macrophage phenotypes during tissue repair. Journal of leukocyte biology. 2013; 93:875–81. [PubMed: 23505314]
21. Daley JM, Brancato SK, Thomay AA, Reichner JS, Albina JE. The phenotype of murine wound macrophages. Journal of leukocyte biology. 2010; 87:59–67. [PubMed: 20052800]
22. Nair MG, Gallagher IJ, Taylor MD, Loke P, Coulson PS, Wilson RA, et al. Chitinase and Fizz family members are a generalized feature of nematode infection with selective upregulation of Ym1 and Fizz1 by antigen-presenting cells. Infect Immun. 2005; 73:385–94. [PubMed: 15618176]

23. Loke P, Gallagher I, Nair MG, Zang X, Brombacher F, Mohrs M, et al. Alternative activation is an innate response to injury that requires CD4+ T cells to be sustained during chronic infection. Journal of immunology. 2007; 179:3926–36.
24. McWhorter FY, Wang T, Nguyen P, Chung T, Liu WF. Modulation of macrophage phenotype by cell shape. Proc Natl Acad Sci U S A. 2013; 110:17253–8. [PubMed: 24101477]
25. Madden LR, Mortisen DJ, Sussman EM, Dupras SK, Fugate JA, Cuy JL, et al. Proangiogenic scaffolds as functional templates for cardiac tissue engineering. Proc Natl Acad Sci U S A. 2010; 107:15211–6. [PubMed: 20696917]
26. Garg K, Pullen NA, Oskeritzian CA, Ryan JJ, Bowlin GL. Macrophage functional polarization (M1/M2) in response to varying fiber and pore dimensions of electrospun scaffolds. Biomaterials. 2013; 34:4439–51. [PubMed: 23515178]
27. Wong VW, Rustad KC, Akaishi S, Sorkin M, Glotzbach JP, Januszyk M, et al. Focal adhesion kinase links mechanical force to skin fibrosis via inflammatory signaling. Nat Med. 2012; 18:148–52. [PubMed: 22157678]
28. Bhalla S, Shiratsuchi H, Craig DH, Basson MD. beta(1)-integrin mediates pressure-stimulated phagocytosis. American journal of surgery. 2009; 198:611–6. [PubMed: 19887187]
29. Ballotta V, Driessen-Mol A, Bouten CV, Baaijens FP. Strain-dependent modulation of macrophage polarization within scaffolds. Biomaterials. 2014; 35:4919–28. [PubMed: 24661551]
30. Amini-Nik S, Cambridge E, Yu W, Guo A, Whetstone H, Nadesan P, et al. β-Catenin-regulated myeloid cell adhesion and migration determine wound healing. The Journal of Clinical Investigation. 2014; 124:2599. [PubMed: 24837430]
31. Graham JS, Vomund AN, Phillips CL, Grandbois M. Structural changes in human type I collagen fibrils investigated by force spectroscopy. Experimental cell research. 2004; 299:335–42. [PubMed: 15350533]
32. Adolph EJ, Hafeman AE, Davidson JM, Nanney LB, Guelcher SA. Injectable polyurethane composite scaffolds delay wound contraction and support cellular infiltration and remodeling in rat excisional wounds. J Biomed Mater Res A. 2012; 100A:450–61. [PubMed: 22105887]
33. Hafeman AE, Zienkiewicz KJ, Zachman AL, Sung HJ, Nanney LB, Davidson JM, et al. Characterization of the degradation mechanisms of lysine-derived aliphatic poly(ester urethane) scaffolds. Biomaterials. 2011; 32:419–29. [PubMed: 20864156]
34. Guelcher SA, Patel V, Gallagher KM, Connolly S, Didier JE, Doctor JS, et al. Synthesis and in vitro biocompatibility of injectable polyurethane foam scaffolds. Tissue Engineering. 2006; 12:1247–59. [PubMed: 16771638]
35. Guelcher S, Srinivasan A, Hafeman A, Gallagher K, Doctor J, Khetan S, et al. Synthesis, In vitro degradation, and mechanical properties of two-component poly(ester urethane)urea scaffolds: Effects of water and polyol composition. Tissue Engineering. 2007; 13:2321–33. [PubMed: 17658992]
36. Dumas JE, Zienkiewicz K, Tanner SA, Prieto EM, Bhattacharyya S, Guelcher S. Synthesis and Characterization of an Injectable Allograft Bone/polymer Composite Bone Void Filler with Tunable Mechanical Properties. Tissue Eng Part A. 2010; 16:2505–18. [PubMed: 20218874]
37. Gibson, LJ.; Ashby, MF. Cellular solids: Structure and properties. Cambridge University Press; 1997.
38. Fonck E, Feigl GG, Fasel J, Sage D, Unser M, Rufenacht DA, et al. Effect of aging on elastin functionality in human cerebral arteries. Stroke. 2009; 40:2552–6. [PubMed: 19478233]
39. Rezakhaniha R, Agianniotis A, Schrauwen JT, Griffa A, Sage D, Bouten CV, et al. Experimental investigation of collagen waviness and orientation in the arterial adventitia using confocal laser scanning microscopy. Biomechanics and modeling in mechanobiology. 2012; 11:461–73. [PubMed: 21744269]
40. Takashima A. Establishment of fibroblast cultures. Current protocols in cell biology / editorial board, Juan S Bonifacino [et al]. 2001 Chapter 2:Unit 2 1.
41. Hafeman A, Li B, Yoshii T, Zienkiewicz K, Davidson J, Guelcher S. Injectable biodegradable polyurethane scaffolds with release of platelet-derived growth factor for tissue repair and regeneration. Pharm Res. 2008; 25:2387–99. [PubMed: 18516665]

42. Quinn KP, Golberg A, Broelsch GF, Khan S, Villiger M, Bouma B, et al. An automated image processing method to quantify collagen fibre organization within cutaneous scar tissue. Experimental dermatology. 2015; 24:78–80. [PubMed: 25256009]
43. Beer HD, Longaker MT, Werner S. Reduced expression of PDGF and PDGF receptors during impaired wound healing. J Invest Dermatol. 1997; 109:132–8. [PubMed: 9242497]
44. El Gazaerly H, Elbardisey DM, Eltokhy HM, Teaama D. Effect of transforming growth factor Beta 1 on wound healing in induced diabetic rats. International journal of health sciences. 2013; 7:160–72. [PubMed: 24421745]
45. Stockmann C, Kirmse S, Helfrich I, Weidemann A, Takeda N, Doedens A, et al. A wound size-dependent effect of myeloid cell-derived vascular endothelial growth factor on wound healing. J Invest Dermatol. 2011; 131:797–801. [PubMed: 21107350]
46. Galeano M, Altavilla D, Cucinotta D, Russo GT, Calo M, Bitto A, et al. Recombinant human erythropoietin stimulates angiogenesis and wound healing in the genetically diabetic mouse. Diabetes. 2004; 53:2509–17. [PubMed: 15331568]
47. Bonanno E, Iurlaro M, Madri JA, Nicosia RF. Type IV collagen modulates angiogenesis and neovessel survival in the rat aorta model. In vitro cellular & developmental biology Animal. 2000; 36:336–40. [PubMed: 10937837]
48. Rustad KC, Wong VW, Gurtner GC. The role of focal adhesion complexes in fibroblast mechanotransduction during scar formation. Differentiation; research in biological diversity. 2013; 86:87–91.
49. Brancato SK, Albina JE. Wound macrophages as key regulators of repair: origin, phenotype, and function. Am J Pathol. 2011; 178:19–25. [PubMed: 21224038]
50. van Putten SM, Ploeger DT, Popa ER, Bank RA. Macrophage phenotypes in the collagen-induced foreign body reaction in rats. Acta Biomater. 2013; 9:6502–10. [PubMed: 23376130]
51. Sephel, GC.; Davidson, JM. Repair, regeneration and fibrosis.. In: Rubin, R.; Strayer, DS., editors. Rubin's Pathology: Clinicopathologic Foundations of Medicine. 6th ed.. Lippincott Williams and Wilkins; Philadelphia, PA: 2012. p. 83-114.
52. Cao H, McHugh K, Chew SY, Anderson JM. The topographical effect of electrospun nanofibrous scaffolds on the in vivo and in vitro foreign body reaction. J Biomed Mater Res A. 2010; 93:1151–9. [PubMed: 19768795]
53. Chong EJ, Phan TT, Lim IJ, Zhang YZ, Bay BH, Ramakrishna S, et al. Evaluation of electrospun PCL/gelatin nanofibrous scaffold for wound healing and layered dermal reconstitution. Acta Biomater. 2007; 3:321–30. [PubMed: 17321811]
54. Adolph EJ, Hafeman AE, Davidson JM, Nanney LB, Guelcher SA. Injectable polyurethane composite scaffolds delay wound contraction and support cellular infiltration and remodeling in rat excisional wounds. Journal of biomedical materials research Part A. 2012:A100A:450–61.
55. Wilgus TA, DiPietro LA. Complex roles for VEGF in dermal wound healing. J Invest Dermatol. 2012; 132:493–4. [PubMed: 22071479]
56. Duscher D, Maan ZN, Wong VW, Rennert RC, Januszyk M, Rodrigues M, et al. Mechanotransduction and fibrosis. J Biomech. 2014; 47:1997–2005. [PubMed: 24709567]
57. Lynch SE, Nixon JC, Colvin RB, Antoniades HN. Role of platelet-derived growth factor in wound healing: Synergistic effects with other growth factors. Proc Natl Acad Sci USA. 1987; 84:7696–700. [PubMed: 3499612]
58. Wipff PJ, Rifkin DB, Meister JJ, Hinz B. Myofibroblast contraction activates latent TGF-beta1 from the extracellular matrix. J Cell Biol. 2007; 179:1311–23. [PubMed: 18086923]
59. Cheon S, Poon R, Yu C, Khoury M, Shenker R, Fish J, et al. Prolonged beta-catenin stabilization and tcf-dependent transcriptional activation in hyperplastic cutaneous wounds. Laboratory investigation; a journal of technical methods and pathology. 2005; 85:416–25.
60. Amini-Nik S, Glancy D, Boimer C, Whetstone H, Keller C, Alman BA. Pax7 expressing cells contribute to dermal wound repair, regulating scar size through a beta-catenin mediated process. Stem Cells. 2011; 29:1371–9. [PubMed: 21739529]
61. Scholzen T, Gerdes J. The Ki-67 protein: from the known and the unknown. J Cell Physiol. 2000; 182:311–22. [PubMed: 10653597]

62. Penn JW, Grobbelaar AO, Rolfe KJ. The role of the TGF-beta family in wound healing, burns and scarring: a review. International journal of burns and trauma. 2012; 2:18–28. [PubMed: 22928164]

63. Lam AP, Gottardi CJ. beta-catenin signaling: a novel mediator of fibrosis and potential therapeutic target. Current opinion in rheumatology. 2011; 23:562–7. [PubMed: 21885974]

64. Cheon SS, Wei Q, Gurung A, Youn A, Bright T, Poon R, et al. Beta-catenin regulates wound size and mediates the effect of TGF-beta in cutaneous healing. FASEB J. 2006; 20:692–701. [PubMed: 16581977]

65. Alfaro MP, Pagni M, Vincent A, Atkinson J, Hill MF, Cates J, et al. The Wnt modulator sFRP2 enhances mesenchymal stem cell engraftment, granulation tissue formation and myocardial repair. Proc Natl Acad Sci U S A. 2008; 105:18366–71. [PubMed: 19017790]

66. Bastakoty D, Saraswati S, Cates J, Lee E, Nanney LB, Young PP. Inhibition of Wnt/β-catenin pathway promotes regenerative repair of cutaneous and cartilage injury. The FASEB Journal. 2015:fj–15.

67. Sindrilaru A, Scharffetter-Kochanek K. Disclosure of the Culprits: Macrophages-Versatile Regulators of Wound Healing. Adv Wound Care (New Rochelle). 2013; 2:357–68. [PubMed: 24587973]

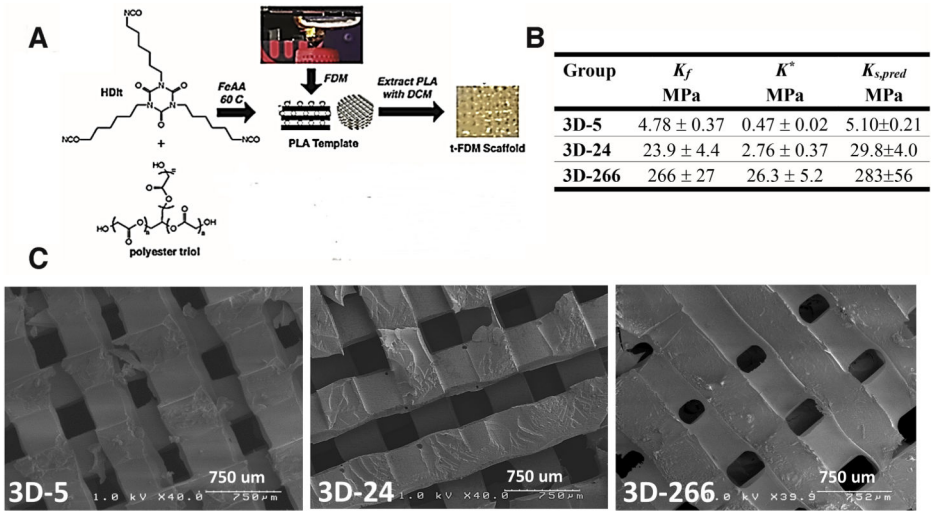

Group	K_f MPa	K^* MPa	$K_{s,pred}$ MPa
3D-5	4.78 ± 0.37	0.47 ± 0.02	5.10±0.21
3D-24	23.9 ± 4.4	2.76 ± 0.37	29.8±4.0
3D-266	266 ± 27	26.3 ± 5.2	283±56

Figure 1. Fabrication and characterization of 3D PUR scaffolds

(A) Process for fabrication of templated 3D scaffolds by Fused Deposition Modeling (t-FDM). The poly(ester urethane) reaction mixture is impregnated into a rectilinear, three-dimensional PLA template that is subsequently leached to produce a porous scaffold with precisely defined architecture. (B) Measured values of the substrate modulus of 2D films (K_f) and the bulk modulus of 3D scaffolds (K^*). The predicted substrate modulus of the polymer in the 3D scaffolds ($K_{s,pred}$) was calculated from the measured bulk modulus of the scaffolds (K^*) using Eq (1). There were no statistically significant differences between K_f and $K_{s,pred}$. (C) SEM images of the t-FDM scaffolds listed in (B).

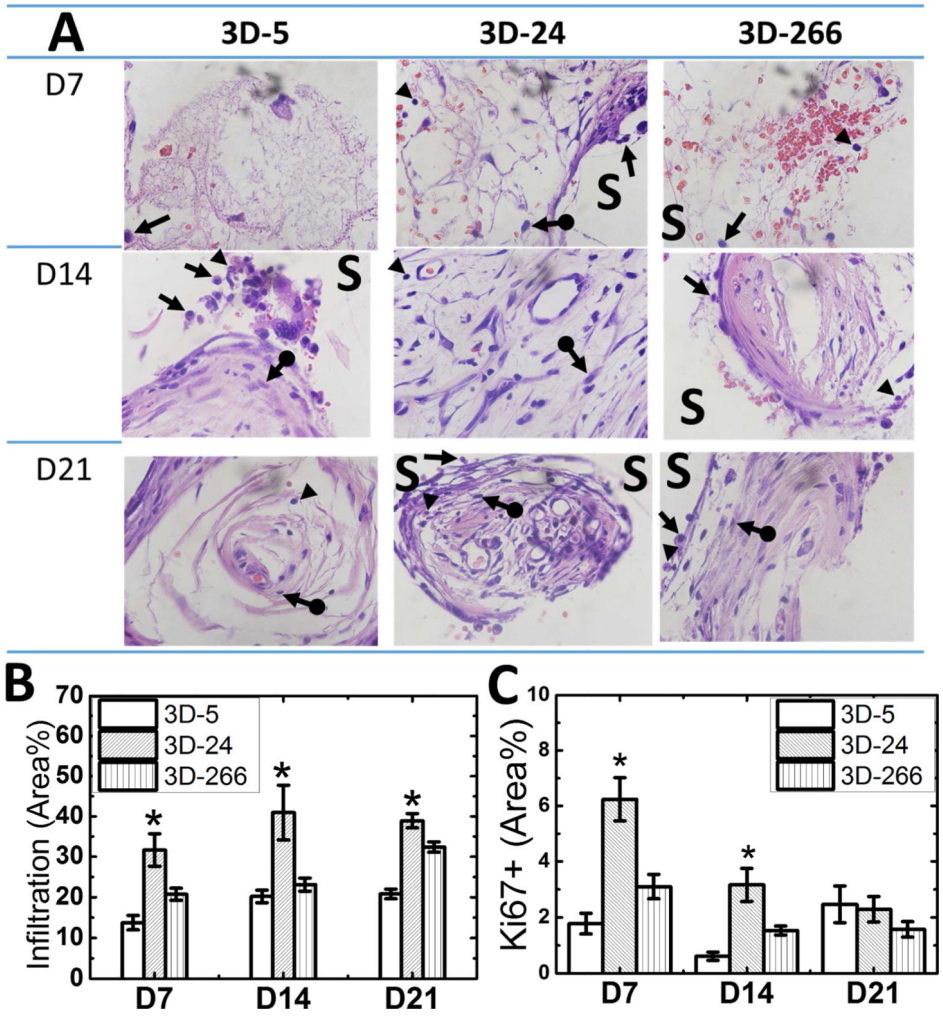

Figure 2. Effects of substrate modulus on cellular infiltration in rat subcutaneous implants

(A) High-magnification images of 3D scaffolds with increasing substrate moduli from tissue harvested on d7, d14, and d21 (100x). Remnants of the scaffold (unstained, S), neutrophils (arrow head) monocytes/macrophages (arrow), and fibroblasts (arrow-dot) were identified based on color and cell morphology. (N=4; *p<0.05) (B) Infiltration of cells into 3D scaffolds measured by histomorphometry. (C) Prevalence of $Ki67^{+}$ cells measured by immunohistochemical staining. (N=4; *p<0.05).

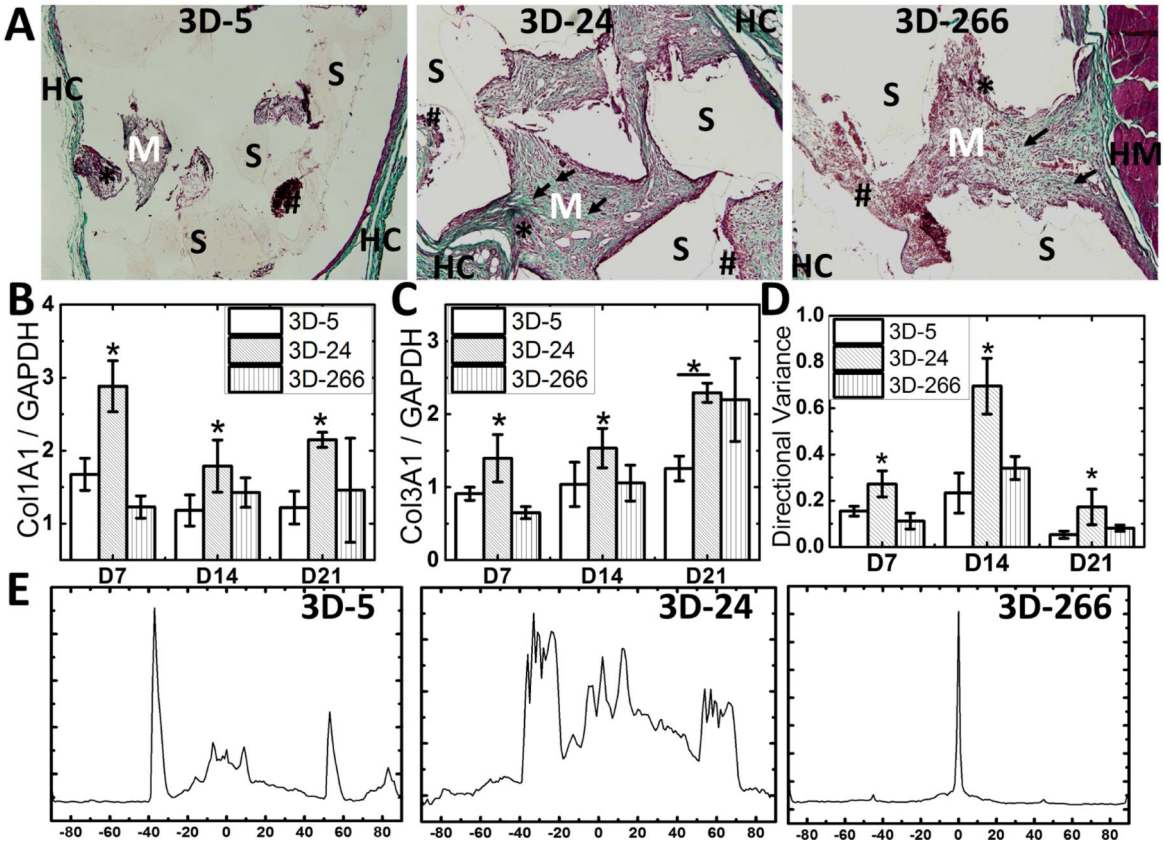

Figure 3. Effects of substrate modulus on collagen deposition in rat subcutaneous implants

(**A**) High-magnification images of histological sections of 3D-5, 3D-24, and 3D-266 scaffolds on d7 stained with trichrome show host collagen (dark green, HC), host muscle (dark red, HM) deposition of new extracellular matrix (emerald green, M) and collagen fibers (arrow), erythrocytes (red, hashtag), cytoplasm of infiltrating cells (pinkish-red, star), and residual scaffold (unstained, S) (20X). Deposition of collagen fibers and new matrix was highest on 3D-24 scaffolds. (**B**) Expression of *Col1A1* (Col-1) and (**C**) *Col3A1* (Col-3) measured by qRTPCR. (**D-E**) Scaffold effects on the orientation of collagen fiber and cells in rat subcutaneous wounds. (**D**) Directional variance of alignment calculated from low-magnification (2x) images of histological sections. Significant differences (N=4; *, $p < 0.05$) were found between either 3D-24 and the other groups at each time point. (**E**) Representative images of Orientation J-generated (Image J) fiber orientation angle distribution.

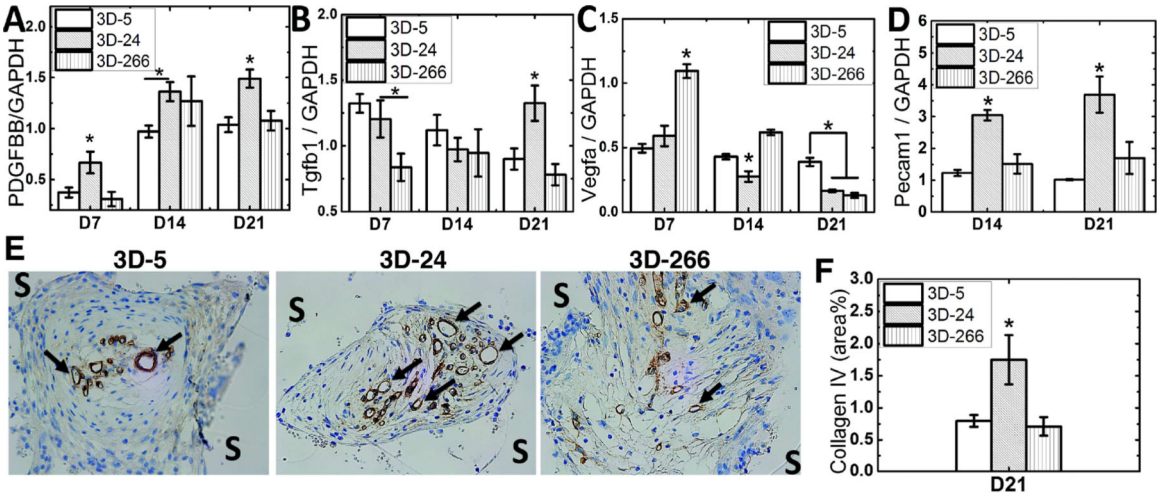

Figure 4. Effects of substrate modulus on scaffold vascularization and expression of growth factors associated with wound healing

(A) Expression of *Pdgfb* was greatest on 3D-24 scaffolds at all time points. (B) Expression of *Tgfb1* was highest on 3D-24 scaffolds on D21. (C) Expression of *Vegfa* was lowest on 3D-24 scaffolds at all time points. (D-G) Wound vascularization, as assessed by (D) *Pecam1* gene expression and (E) immunohistochemical staining of collagen IV (40X), was highest in 3D-24 scaffolds on d21. Arrows differentiate positive staining for collagen IV (COLIV) associated with neovessel formation from background. (F) Quantification of $COLIV^{+}$ staining by histomorphometry (N=4; *$p<0.05$).

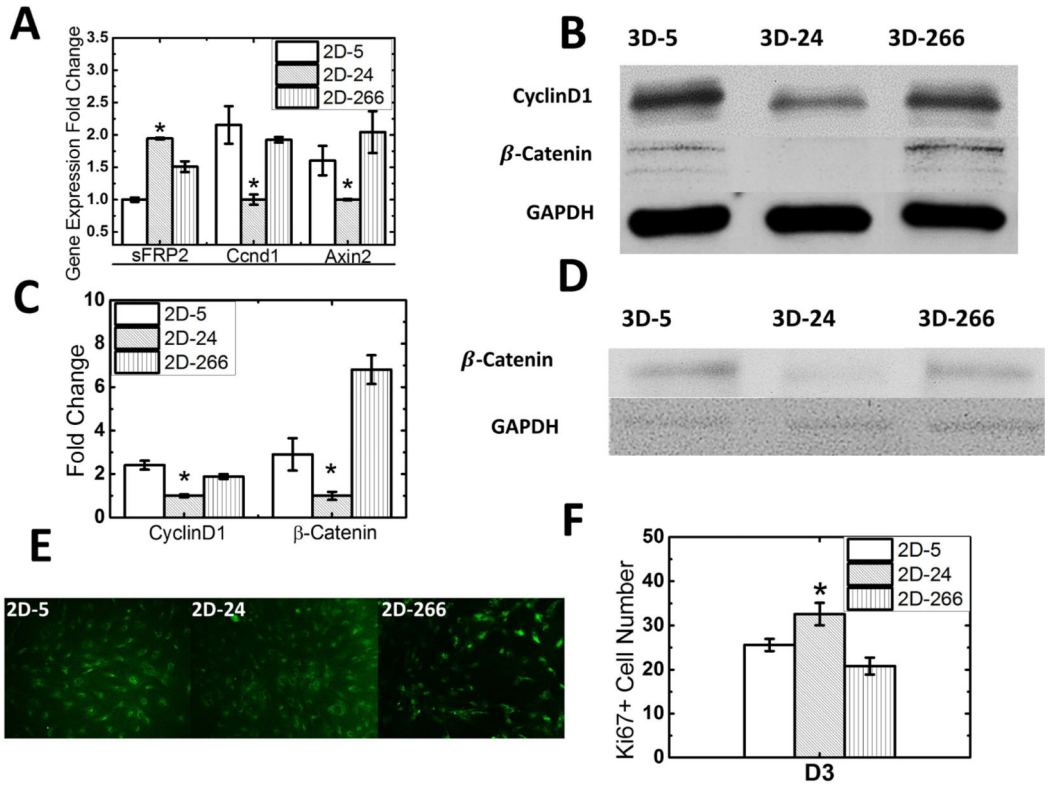

Figure 5. Effects of substrate modulus on Wnt signaling in fibroblasts

(A) Expression of Wnt target genes *Ccd1* and *Axin2* by fibroblasts harvested from granulation tissue was down-regulated on 3D-24 scaffolds, while expression of the Wnt inhibitor *sFRP2* was up-regulated. (B, C) Fibroblasts from granulation tissue were cultured on 2D-5, 2D-24 and 2D-266 substrates. Protein expression level of β-catenin, an intracellular signal transducer in the Wnt signaling pathway, as well as its target protein Cyclin D1 were lowest on 3D-24 scaffolds in harvested fibroblasts. (D) Protein expression level of β-catenin from dermal fibroblasts was also lowest on 3D-24 scaffolds which was consistent with granulation tissue fibroblasts. GAPDH was shown as a control for protein loading. (E) Immunofluorescence images (20X) of granulation tissue fibroblasts cultured on 2D films and stained for Ki67 showed the highest number of cells after 3 days culture on 2D-24. (F) The mean number of cell counts averaged from six fields of view at 40X magnification (as shown in Panel E) on d3 is highest on 2D-24 films.

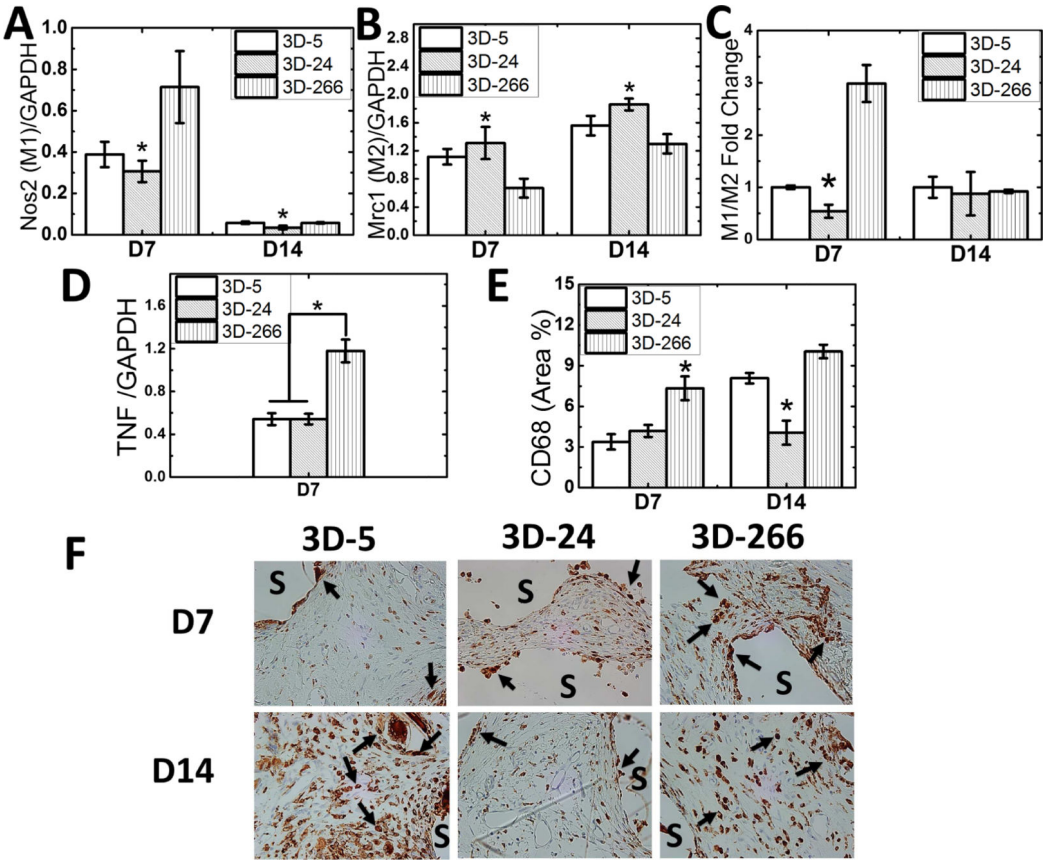

Figure 6. Effects of substrate modulus on macrophage polarization

(A) Expression of the M1 marker iNOS (*Nos2*) was significantly lower on 3D-24 scaffolds on d7. (B) Expression of the M2 marker CD206 (*Mrc1*) was significantly higher on 3D-24 scaffolds on d7 and d14. (C) M1/M2 ratio was lowest on 3D-24 scaffolds on d7. (D) Expression of the M1 marker TNF-α (*Tnf*) was lower on 3D-5 and 3D-24 scaffolds on d7. (E) The total number of macrophages, as assessed by CD68 immunohistochemical staining, was lowest on 3D-5 and 3D-24 scaffolds. (F) Representative high magnification (40X) images of CD68 immunohistochemical staining. Arrows show positively-stained macrophages, which are concentrated near the surface of the scaffold (S).

Table 1

Animal study design.

Treatment group	Polyester triol M_n (g/mol)	*K* MPa	7 days	14 days	21 days
3D-5	3000	5	4	4	4
3D-24	720	24	4	4	4
3D-266	300	266	4	4	4

Table 2

Primers used for qPCR analysis.

Gene	Forward 5’ to 3’	Reverse 5’ to 3’
PDGFBB	CCCACACGTCAAACTACAGCTCCAA	GCCCAGTTCGTTTCAGTGCCACAT
CollA1	TGCTGATGGACAACCTGG	ACTGTTGCCTTTGGGACC
Col3A1	CTGGATCTCCTGGTGCTAAG	CAGCGTGTCCTTGTGGTC
Pecam1	GGAGGTGACAGAAGGTGGGATTG	GCTTGGCAGCGAAACACTAACAGG
Vegfa	GCCAGCACATAGGAGAGATGAG	ACCGCCTTGGCTTGTCAC
Tgfb	AAGTGGATCCACGAGCCCAA	GCTGCACTTGCAGGAGCGCA
TNF	GGCCACCACGCTCTTTCTGTCA	TGGGCTACGGGCTTGTCACTC
Nos2	CCTGGTGCAAGGGATCTTGG	GAGGGCTTGCCTGAGTGAGC
Mrc1	GGTTCCGGTTTGTGGAGCAG	TCCGTTTGCATTGCCCAGTA
GAPDH	GACTTCAACAGCAACTCC	GCCATATTCATTGTCATACCA
Axin2	GGACAGTAGCGTAGATGGAG	CGGAAAATGAGGTAGAGACA
Ccnd1	CTGGTGTTTGGAAGTAGGAA	GTTTAAAAGCCTCCTGTGTG
sFRP2	ATGGAAACCCTTTGTAAAAATGACT	TCTTGCTCTTTGTCTCCAGGATGAT